Ab Initio and Density Functional Study of the Electronic Transitions of Indoline and Indoline-2-Carboxylic Acid

Brian D. Slaughter, Michael W. Allen, G. H. Lushington, and Carey K. Johnson*

Department of Chemistry, University of Kansas, Lawrence, Kansas 66045

Received: December 23, 2002; In Final Form: May 6, 2003

In this study, a range of computational methods including time-dependent density functional theory, configuration interaction, and Zerner's spectroscopic intermediate neglect of differential overlap are used to classify spectroscopic properties of indoline and indoline-2-carboxylic acid. By examining transition densities, the ^1L_a and ^1L_b states of indoline and indoline-2-carboxylic acid are assigned. Aniline is used as a reference system. Excitation energies, oscillator strengths, dipole moments, and transition dipoles have been calculated and are found to be in close agreement with experiment. We find that the electronic transitions of indoline are similar to those for aniline. The lowest excited singlet state in indoline, as in aniline, is the ^1L_b state with a low oscillator strength. The ^1L_a state is higher in energy and possesses a larger oscillator strength as well as a larger dipole moment. For indoline-2-carboxylic acid, ^1L_b- and ^1L_a-like states can be identified, but an evaluation of their properties reveals mixed ^1L_a and ^1L_b character. Ground-state energies for conformations of indoline-2-carboxylic acid differing in the orientation of the carboxylic group indicate the presence of two ground-state conformations of similar energy.

Introduction

A range of computational methods including configuration interaction (CI), Møller−Plesset perturbation theory (MP2), and density functional theory (DFT) have made increasingly important contributions to our understanding of molecular systems.[1−3] The availability of a range of computational tools affords the experimental chemist the opportunity to use computational methods hand-in-hand with experiment to understand the spectroscopic properties of molecules. In particular, recent developments in time-dependent density functional theory (TDDFT) now extend the computational efficiency and accuracy of DFT to the calculation of excited-state properties.[4,5]

In this paper, we apply methods of computational chemistry as tools to understand the spectroscopic properties of indoline and its derivative, indoline-2-carboxylic acid (I2CA) (Figure 1). Indoline is an aromatic amine, closely related to indole, the fluorescent side chain of the aromatic amino acid tryptophan, but lacking the C2═C3 double bond present in indole. I2CA is an amino acid and can be regarded as a derivative of proline with a fused phenyl group. Recently, we have employed I2CA as a fluorescent proline analogue, substituting it for proline in several short-chain peptides.[6,7] In this paper, we undertake a theoretical study of the spectroscopic properties of indoline and I2CA. A companion paper[8] describes an experimental study of the spectroscopy and photophysics of these molecules. A third manuscript will describe the properties of peptides containing I2CA as a substitute for proline.[9]

The study of peptide dynamics by fluorescence requires either the detection of fluorescence from a native amino acid or the attachment of an extrinsic fluorescent label. The natural amino acids tyrosine, tryptophan, and phenylalanine are limited in their excitation wavelength ranges and in their quantum yields. The amino acid having the highest fluorescence yield of the native amino acids, tryptophan, is further beset by complications due to overlapping electronic states (^1L_a and ^1L_b states). For these reasons, the search is ongoing to improve quantum yield or expand the wavelength range with minimum perturbation to peptides or proteins.[10]

The substitution of indoline into peptides aids in the determination of reorientational properties of peptides in solution by time-resolved fluorescence depolarization measurements. I2CA differs from tyrosine, tryptophan, and phenylalanine in that, like proline, its ring structure is rigidly attached to the peptide backbone. Consequently, the transition dipole of indoline is strongly coupled to the peptide backbone. Changes in the anisotropy of indoline are therefore directly related to the motion of the peptide backbone without the possibility of free rotation of the fluorophore. In contrast, a component is present in the anisotropic decay of tyrosine, tryptophan, or phenylalanine that is due to the rotational freedom of the fluorophore.

It is our goal in this paper to characterize the lowest-energy spectroscopic transitions of indoline and I2CA. As an aromatic fluorophore, indoline and its derivatives possess electronic states related to those of other aromatics. Electronic transitions for indoline at 287 and 237 nm appear to correspond to similar transitions of aniline.[8] The absorption spectrum of I2CA appears to be more congested but superficially resembles that of indoline. It is common to name the two lowest π to π^* transitions for aromatic molecules as ^1L_a and ^1L_b, following Platt's nomenclature.[11,12] Recent theoretical work involving these transitions has been reported for indole, the fluorophore of tryptophan, examining the overlapping ^1L_a and ^1L_b transitions.[13−18]

The ^1L_a and ^1L_b states are distinguished by the pattern of nodes in the electronic wave function. For the ^1L_b state, nodes in the wave function pass through the atoms of the aromatic ring, and transition density is centered between these atoms.[12] In contrast, for the ^1L_a state, nodes pass between atoms of the aromatic; consequently, the transition density for the ^1L_a state is centered on the atoms. The ^1L_a state has a larger dipole

* Corresponding author. E-mail: ckjohnson@ku.edu.

10.1021/jp027814h CCC: $25.00
Published on Web 07/02/2003

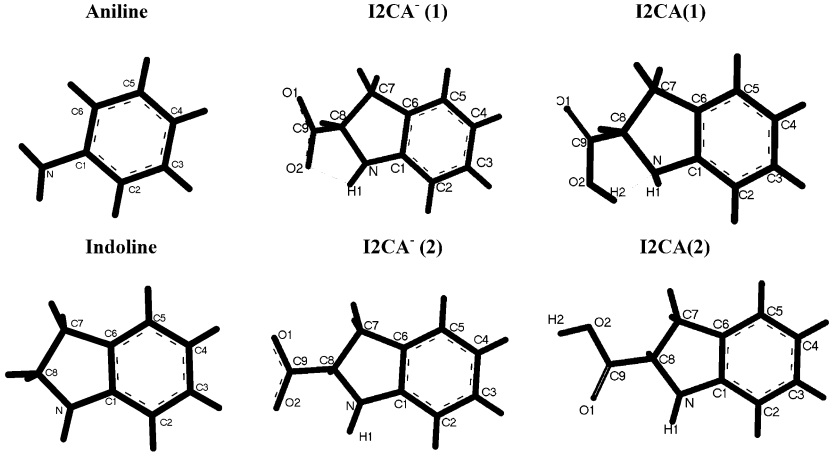

Figure 1. MP2/6-31G* optimized structures of aniline, indoline, I2CA$^-$ (1), I2CA$^-$ (2), I2CA(1), and I2CA(2).

moment and stronger absorption bands and is more susceptible to shifts by atom substitutions and changes in solvent polarity. The ^1L_b state, in contrast, is characterized by a relatively weak dipole moment, lower relative oscillator strength, and little response to shifts in solvent polarity.

The determination of which state has the lowest energy is of particular importance for understanding the fluorescence properties of indoline and I2CA. These properties depend on whether the fluorescence originates from a ^1L_a or ^1L_b state or whether the two states lie in close proximity to each other, as in indoles. The quantum calculations reported here allow us to assign the ^1L_a and ^1L_b electronic transitions of indoline and I2CA using a number of different theoretical methods. Configuration interaction involving single excitations (CIS)[1] was used. Semiempirical calculations were carried out with the spectroscopically parametrized intermediate neglect of differential overlap as written by Zerner (ZINDO).[19−21] Also used was TDDFT,[22−24] which allows for the rigorous inclusion of Coulomb correlation effects into state energetics at no considerable extra computational cost relative to that of CIS. TDDFT has become increasingly valuable for obtaining theoretical excitation energies and spectroscopic transition properties. In particular, the recent addition of more extensive functionals has led to significant enhancements in TDDFT.[25]

Methods

All calculations were made using the software package Gaussian 98.[26] Optimized ground-state geometries of indoline and I2CA were obtained at the MP2 level of theory with the 6-31G* basis set.[27] In each case, all molecular degrees of freedom were optimized. MP2 optimizations have consistently been shown to predict bond lengths within 0.015 Å and angles within 0.3° for small organic molecules.[3] Structures for which hydrogen bonding was predicted were also optimized with the 6-31G**[27] basis set. The inclusion of the additional polarization functions may increase the accuracy of the prediction of the presence of hydrogen bonds.

Excited-state energies and oscillator strengths for these systems were obtained using a variety of different methods including the ZINDO implementation of the INDO-S method, configuration interaction with single excitations (CIS), and the time-dependent density functional (TDDFT) method, all as implemented in Gaussian 98.[26] For the excited-state expansions of aniline and indoline, the first two predicted excited states were treated. In the case of the various forms of I2CA, transition densities and orbitals were used to identify the L_a and L_b transitions. Roots representing these transitions were specified for further calculations. In the ZINDO-level treatment, all other parameters were left at their default values as implemented in Gaussian. For CIS, the excited-state expansions were effected over the full set of valence and virtual Hartree−Fock-level molecular orbitals as generated at a variety of different basis set levels (6-31G[28] and 6-31G*[27]), and all other parameters were left at their default values. In the TDDFT case, similar basis sets were employed, the BLYP[29] and B3LYP[30] exchange-correlation functionals were compared, and default settings were retained for all additional parameters. In addition to the excitation energy and oscillator strength calculations, transition density distributions were obtained for selected states of interest using the TDDFT method at the BLYP/6-31G* level. The distributions were plotted over a 3D grid of size and density determined by the default settings of the Gaussian CUBE utility. All other TDDFT settings were also left at their default values for these calculations. Molecular orbitals involved in the transition were imaged using Molden.[31] Transition densities and transition dipoles were imaged using gOpenMol.[32,33]

Absorption Spectra. Aniline (99%), indoline (99%), and indoline-2-carboxylic acid (97%) were obtained from Aldrich. Aniline was purified by distillation before use. Absorption spectra of aniline and indoline in water were taken with a Cary 50 spectrophotometer. A water background spectrum was used as a reference. Absorption spectra of I2CA were taken in water and in acetonitrile. In water, the pH was adjusted to 7.0 by the addition of 0.1 M NaOH. Low pH absorption spectra of aniline, indoline, and I2CA (not shown) were obtained by the addition of dilute HCl.[8]

The absorption curve of each absorption spectrum was fit to a sum of 4 or 5 log-normal functions[34] to resolve the contributions of the ^1L_a, ^1L_b, and ^1B bands to the total absorption. Log-normal functions have been shown to be successful in resolving the contributions of different bands when an overlap between the bands exists and are effective for representing the skewed property of absorption bands toward higher wavenumbers.[34−36] The use of three log-normal functions, one each for the ^1L_b, ^1L_a, and ^1B features in the absorption spectra, was not sufficient to reproduce the entire absorption spectra accurately. The addition of a small-magnitude function was required between the ^1L_a and ^1B peak. In the case of indoline and I2CA, four log-normal functions accurately reproduced the absorption spectra. The accurate fit of the absorption spectra of aniline required the addition of a function in the $^1L_b-{}^1L_a$ gap in addition to one in the $^1L_a-{}^1B$ gap. Integration under each curve was

TABLE 1: Ground-State MP2/6-31G* Optimized Bond Lengths and Dihedral Angles

Bond Lengths (Å)

I2CA$^-$ (1)		I2CA$^-$ (2)		I2CA(1)		I2CA(2)		indoline		aniline	
C1−C2	1.399	C1−C2	1.400	C1−C2	1.392	C1−C2	1.393	C1− C2	1.394	C1−C2	1.402
C1−N	1.400	C1−N	1.376	C1−N	1.435	C1−N	1.407	C1−N	1.409	C1−N	1.407
C1−C6	1.408	C1−C6	1.418	C1−C6	1.399	C1−C6	1.404	C1−C6	1.402	C1−C6	1.402
C2−C3	1.399	C2−C3	1.401	C2−C3	1.398	C2−C3	1.400	C2−C3	1.400	C2−C3	1.394
C3−C4	1.399	C3−C4	1.397	C3−C4	1.400	C3−C4	1.398	C3−C4	1.398	C3−C4	1.396
C4−C5	1.402	C4−C5	1.406	C4−C5	1.399	C4−C5	1.401	C4−C5	1.401	C4−C5	1.396
C5−C6	1.391	C5−C6	1.387	C5−C6	1.393	C5−C6	1.389	C5−C6	1.390	C5−C6	1.394
C6−C7	1.506	C6−C7	1.513	C6−C7	1.508	C6−C7	1.509	C6−C7	1.509		
N−C8	1.487	N−C8	1.476	N−C8	1.485	N−C8	1.464	N−C8	1.476		
C7−C8	1.539	C7−C8	1.532	C7−C8	1.541	C7−C8	1.541	C7−C8	1.537		
C8−C9	1.570	C8−C9	1.550	C8−C9	1.539	C8−C9	1.508				
C9−O1	1.258	C9−O1	1.260	C9−O1	1.217	C9−O1	1.217				
C9−O2	1.268	C9−O2	1.266	C9−O2	1.343	C9−O2	1.360				

Dihedral Angles[a] (deg)

I2CA$^-$ (1)		I2CA$^-$ (2)		I2CA(1)		I2CA(2)		indoline		aniline	
D1	−20.6	D1	−57.4	D1	−136.7	D1	−71.1				
D2	2.6	D2	−3.0	D2	−1.8	D2	−3.1	D2	−2.7	D2	4.0
D3	19.5	D3	43.8	D3	14.9	D3	−161.4				

[a] D1 is the dihedral angle H1−N−C8−C9. D2 is the dihedral angle H−C2−C1−N. D3 is the dihedral angle N−C8−C9−O2.

carried out. The areas under the curves of the additional log-normal functions were incorporated with the areas for the functions to smaller wavenumbers. The sum of the areas was then used to calculate the oscillator strength for the absorption feature using the equation $f = 4.32 \times 10^{-9} * \int \epsilon(\nu)\, d\nu$.[37]

Results and Discussion

Ground-State Calculations. Molecular Geometry. Optimized MP2/6-31G* ground-state geometries for aniline, indoline, and I2CA are shown in Figure 1. Optimized parameters are in Table 1. The MP2/6-31G* structure of aniline has been calculated previously.[38]

Two ground-state structures, predicted to be within 4 kcal/mol of one another, were found for I2CA in the negatively charged form with a carboxylate anion, expected in aqueous solution at neutral pH. The most dramatic difference between the two is the dihedral angle formed by H1−N−C8−C9 (Table 1). For the lowest-energy structure, termed I2CA$^-$ (1), this angle is −20.6°, and the angle for the second conformer, I2CA$^-$ (2), is −57.4°. The lower value of this dihedral angle in I2CA$^-$ (1) and the location of H1 and C9 out of the plane of the aromatic allows for a hydrogen bond to form. This proposed intramolecular hydrogen bond is formed over a 2.0-Å distance. The larger dihedral angle formed by H1−N−C8−C9 in I2CA$^-$ (2) prevents the formation of this hydrogen bond.

Two ground-state structures were also found for the neutral form of I2CA. These two neutral structures are shown in Figure 1 as I2CA(1) and I2CA(2) and are calculated to have energies within 1 kcal/mol of one another. Similar to the case of I2CA in water, an intramolecular hydrogen bond is mainly responsible for the difference between the two. For the lower-energy structure, I2CA(1), a hydrogen bond is formed between N and H2, which are separated by less than 2.0 Å. This hydrogen bond can be formed because of the proximity of the N−C8−C9−O2 dihedral (14.9°) to 0° in I2CA(1), allowing H2 to move close to the nitrogen. For I2CA(2), this dihedral is −161.4°. The presence of the hydrogen bond may explain the presence of the shorter of the two fluorescence lifetimes of I2CA in nonaqueous solution.[8] The presence of this hydrogen bond was further substantiated by optimizing the I2CA structures with the 6-31G** basis. Structures were not significantly changed with the increase in basis set size.

For aniline, indoline, and the acid structures, the MP2 level of theory predicts a nonplanar geometry between the benzene ring and the nitrogen atom. The dihedral angle defined by H−C2−C1−N measures the nonplanarity of the nitrogen relative to the aromatic ring. MP2 predicts this angle to be 4.0° for aniline, with values ranging from 1.8 to 3.3° for the other structures. A nonplanar nitrogen has been observed in aniline by X-ray crystallography,[39] which found an out-of-plane angle of 4.6°. Hartree−Fock calculations of aniline have predicted this angle to be between 2 and 3.1°[40] depending on the basis set used.

The changes in the MP2 ground-state geometry for the acid structures compared to aniline and indoline are most pronounced with the C1−C6 bond and the C1−N bond (Figure 1 and Table 1). The C1−N bond is 1.376 Å for I2CA$^-$ (2) and 1.435 Å for I2CA(1) compared to 1.407 and 1.409 Å for aniline and indoline, respectively. The C1−N bond in I2CA$^-$ (1) is 1.400 Å, a value closer to that of aniline and indoline than to that of I2CA$^-$ (2). The C1−C6 bond for I2CA$^-$ (2) is 0.016 Å longer than this bond for aniline and indoline. The N−C8 bond lengthens for I2CA(1) to 1.485 Å.

Structures for the low pH form of aniline, indoline, and I2CA$^-$ (1) were also determined with the MP2 level of theory (not shown). The positive charge on the nitrogen in these structures results in a lengthening of the C1−N bond by 0.083, 0.076, and 0.12 Å for aniline, indoline, and I2CA$^-$ (1), respectively, relative to that of the neutral pH structure.

Ground-State Dipole Moment. The ground-state MP2 geometry was used to calculate the ground-state dipole moment. For aniline, the ground-state DFT dipole moment calculated with the BLYP functional and the 6-31G* basis was 1.73 D, which compares well with a previous value calculated using a DFT/BLYP optimized geometry (1.78 D).[38] The experimental dipole moment has been reported as 1.53 D.[41]

The calculated ground-state dipole moment for indoline was 1.46 D. I2CA$^-$ (1) has a ground-state dipole moment of 7.76 D compared to 9.83 D for I2CA$^-$ (2). The neutral I2CA structures have dipole moments of 4.96 and 1.74 D for the hydrogen-bonded and non-hydrogen-bonded structures, respectively. Values for ground- and excited-state dipole moments are tabulated in Table 4.

TABLE 2: Experimental, Semiempirical, CIS, and TDDFT Transition Energies for the ^1L_a, ^1L_b, and ^1B Electronic Transitions[a]

	transition energy (eV)									
	B3LYP			BLYP			CIS			
	6-31G	6-31G*	6-31G**	6-31G	6-31G*	6-31G**	6-31G	6-31G*	ZINDO	exptl
aniline										
$^1A-^1L_b$	4.946	4.935	4.925	4.549	4.566	4.557	6.098	5.975	4.450	4.428
$^1A-^1L_a$	5.869	5.793	5.786	5.568	5.512	5.506	6.445	6.303	5.416	5.391
$^1A-^1B$	7.089	6.996	6.986	6.853	6.760	6.751	8.390	8.078	6.400	6.326
indoline										
$^1A-^1L_b$	4.718	4.698	4.690	4.278	4.286	4.271	5.977	5.841	4.347	4.320
$^1A-^1L_a$	5.567	5.507	5.498	5.221	5.178	5.167	6.308	6.167	5.265	5.232
$^1A-^1B$	6.795	6.710	6.707	6.492	6.387	6.778	7.997	7.926	6.289	6.168
I2CA$^-$ (1)										
$^1A-^1L_b$	4.783	4.728	4.719	4.177	4.162	4.150	5.874	5.741	4.295	4.305
$^1A-^1L_a$	5.550	5.479	5.469	5.106	5.041	5.033	6.234	6.101	5.071	5.232
$^1A-^1B$	6.765	6.648	6.638	6.465	6.329	6.319	7.919	7.825	6.322	6.168
I2CA$^-$ (2)										
$^1A-^1L_b$	4.435	4.385	4.382	3.961	3.928	3.919	5.701	5.572	4.178	4.305
$^1A-^1L_a$	5.266	5.199	5.188	4.907	4.858	4.845	6.086	5.972	4.834	5.232
$^1A-^1B$	6.793	6.650	6.641	6.489	6.511	6.500	7.872	7.775	6.060	6.168
I2CA(2)										
$^1A-^1L_b$	4.769	4.757	4.751	4.336	4.330	4.322	5.985	5.844	4.351	4.217
$^1A-^1L_a$	5.587	5.521	5.511	5.270	5.200	5.191	6.304	6.163	5.307	5.145
$^1A-^1B$	6.821	6.686	6.666	6.537	6.424	6.415	8.048	7.935	6.265	6.108
I2CA(1)										
$^1A-1$	4.996	4.971	4.964	4.350	4.328	4.321	6.203	6.037	4.445	4.217
$^1A-2$	5.286	5.389	5.388	4.765	4.725	4.717	6.414	6.240	5.511	5.145
$^1A-3$	5.708	5.648	5.643	4.782	4.823	4.819	8.112	8.002	6.306	6.108
$^1A-4$	5.859	5.927	5.924	5.014	5.019	5.016				
$^1A-^1B$	6.824	6.761	6.752	6.481	6.399	6.392				

[a] Experimental values for the acid structures are weighted averages of the all the conformers present. The average experimental values are compared to the theoretical values for each structure.

TABLE 3: Experimental, Semiempirical, CIS, and TDDFT Oscillator Strengths for the ^1L_a, ^1L_b, and ^1B Electronic Transitions[a]

	oscillator strength (au)									
	B3LYP			BLYP			CIS			
	6-31G	6-31G*	6-31G**	6-31G	6-31G*	6-31G**	6-31G	6-31G*	ZINDO	exptl
aniline										
$^1A-^1L_b$	0.032	0.030	0.031	0.026	0.025	0.025	0.054	0.050	0.024	0.026
$^1A-^1L_a$	0.162	0.131	0.131	0.161	0.138	0.138	0.047	0.039	0.254	0.157
$^1A-^1B$	0.557	0.524	0.518	0.479	0.455	0.440	1.023	0.607	0.780	0.421
indoline										
$^1A-^1L_b$	0.045	0.045	0.046	0.033	0.034	0.035	0.078	0.077	0.031	0.049
$^1A-^1L_a$	0.130	0.103	0.103	0.130	0.107	0.108	0.034	0.027	0.221	0.157
$^1A-^1B$	0.479	0.375	0.327	0.301	0.361	0.362	0.778	1.008	0.630	0.447
I2CA$^-$ (1)										
$^1A-^1L_b$	0.074	0.074	0.075	0.047	0.049	0.049	0.093	0.093	0.041	0.056
$^1A-^1L_a$	0.089	0.086	0.086	0.089	0.102	0.086	0.058	0.048	0.225	0.161
$^1A-^1B$	0.373	0.447	0.448	0.149	0.282	0.286	0.982	0.996	0.455	0.506
I2CA$^-$ (2)										
$^1A-^1L_b$	0.034	0.053	0.053	0.043	0.042	0.043	0.106	0.104	0.057	0.056
$^1A-^1L_a$	0.164	0.149	0.149	0.144	0.141	0.142	0.119	0.106	0.260	0.161
$^1A-^1B$	0.272	0.413	0.358	0.201	0.202	0.205	1.013	1.038	0.408	0.506
I2CA(2)										
$^1A-^1L_b$	0.040	0.032	0.031	0.031	0.031	0.032	0.073	0.074	0.028	0.056
$^1A-^1L_a$	0.082	0.100	0.100	0.083	0.108	0.109	0.032	0.028	0.209	0.164
$^1A-^1B$	0.400	0.412	0.400	0.401	0.440	0.446	1.027	1.072	0.884	0.466
I2CA(1)										
$^1A-1$	0.025	0.032	0.032	0.012	0.011	0.011	0.033	0.038	0.014	0.056
$^1A-2$	0.006	0.001	0.011	0.017	0.010	0.009	0.004	0.003	0.139	0.164
$^1A-3$	0.077	0.062	0.061	0.042	0.037	0.039	1.023	1.050	0.791	0.466
$^1A-4$	0.003	0.009	0.009	0.008	0.017	0.015				
$^1A-^1B$	0.244	0.278	0.282	0.202	0.210	0.217				

[a] Experimental values for the acid structures are weighted averages of the all the conformers present. The average experimental values are compared to the theoretical values for each structure.

Molecular Orbitals. The HOMO−1, HOMO, LUMO, and LUMO+1 orbitals for aniline, indoline, and I2CA (Figure 2) have been calculated by the BLYP functional and the 6-31G* basis. The nodal patterns of these orbitals show a number of similarities from one molecule to the next. A common trend is the node passing between carbon atoms C2 and C3 and also between C5 and C6 for the HOMO and LUMO orbitals. (See Figure 1 for atom numbering.) This trend does not hold as

TABLE 4: Dipole Moments for the Ground, L_b, and ^1L_a States Calculated by the BLYP Functional and the 6-31G* Basis along with Transition Configurations and Oscillator Strengths from BLYP/6-31G**

	configuration	coeff	DM (D)	osc str BLYP (exptl) (au)
aniline				
^1L_b	HOMO−LUMO	0.62806	1.69	0.025(0.026)
	HOMO−1 LUMO+1	0.25271		
^1L_a	HOMO−LUMO+1	0.57782	3.63	0.138(0.157)
	HOMO−1 LUMO	−0.25035		
G. S.			1.73	
indoline				
^1L_b	HOMO−LUMO	0.63920	1.55	0.035(0.049)
	HOMO−1 LUMO+1	0.21042		
^1L_a	HOMO−LUMO+1	0.59862	2.05	0.108(0.157)
	HOMO−1 LUMO	−0.20958		
G. S.			1.46	
$I2CA^-$ (1)				
^1L_b	HOMO−LUMO	0.6409	2.47	0.049(0.056)
	HOMO−1 LUMO+1	0.1726		
^1L_a	HOMO−LUMO+1	0.5237	3.30	0.086(0.161)
	HOMO−1 LUMO	−0.1751		
G. S.			7.76	
$I2CA^-$ (2)				
^1L_b	HOMO−LUMO	0.6440	2.37	0.043(0.056)
	HOMO−1 LUMO+1	−0.1509		
^1L_a	HOMO−LUMO+1	0.5831	3.94	0.142(0.161)
	HOMO−1 LUMO	0.1885		
G. S.			9.83	
I2CA(2)				
^1L_b	HOMO−LUMO	0.6319	1.95	0.031(0.056)
	HOMO−1 LUMO+1	−0.2124		
^1L_a	HOMO−LUMO+1	0.5931	3.31	0.109(0.164)
	HOMO−1 LUMO	0.2207		
G. S.			1.74	
I2CA(1)				
trans 1			1.15	0.011
trans 2	HOMO−LUMO	0.5075	1.03	0.009
trans 3			2.04	0.039
trans 4	HOMO−LUMO+1	0.5664	1.32	0.015
G. S.			4.96	

strongly for the neutral acid structures. The HOMO−1 and LUMO+1 orbitals differ in that there is no node present along these bonds, but rather the nodes seem to be shifted along the C2−C5 axis for the H-1 orbitals and between the C1−C2, C3−C4, C4−C5, and C6−C1 bonds for the LUMO+1 orbitals. Again, the neutral acid structures do not hold as strongly to this trend.

In the case of the acid structures, there are additional π orbitals present that contain density that is centered mostly on the carboxyl group (not shown). A number of these occupied orbitals are higher in energy than the orbitals shown. However, these orbitals contribute to electronic transitions with predicted oscillator strengths so small (generally less than 0.001) that they are not seen spectroscopically. The orbitals shown for I2CA are analogous to the HOMO−1, HOMO, LUMO, and LUMO+1 orbitals of indoline and aniline and are the orbitals involved in the ^1L_a and ^1L_b transitions.

Excited States. Experimental Absorption Spectra. The absorption spectra of indoline and I2CA are very similar to that of aniline (Figure 3). In water, the ^1L_b and ^1L_a states of aniline absorb at 280 and 230 nm, respectively. Indoline has peaks in the absorbance spectrum at 287 and 237 nm, and I2CA absorbs at 288 and 237 nm. In acetonitrile, the peaks are slightly red-shifted to 294 and 241 nm.[8] In Figure 3, an increase in the ^1L_b extinction coefficient in going from aniline to indoline to I2CA is evident. There is a significant decrease in the ^1L_a extinction coefficient in indoline and I2CA compared to that in aniline, along with a broadening of the ^1L_a absorption feature in indoline and I2CA. Both absorption features of indoline and I2CA are red-shifted relative to those of aniline. This is in contrast to the UV absorption spectrum of tryptophan (not shown), which has no sharp feature at 235 nm and contains a broad band centered at 280 nm consisting of the overlapping of the ^1L_a and ^1L_b bands.

In aqueous solution at low pH, the ^1L_a and ^1L_b absorption features of aniline and indoline are replaced by two weak absorption features near 260 nm (not shown).[8] TDDFT predicts this significant lowering of oscillator strength for the low pH structures, presumably caused by the loss of resonance between the nitrogen and the aromatic ring, as indicated by the lengthening of the C1−N bond.

Excitation Energies. Vertical excitation energies were calculated by TDDFT with the B3LYP and BLYP functionals, CIS, and ZINDO and are listed in Table 2 along with experimental values. A summary of the results for each method is shown in Figure 4 for aniline, indoline, $I2CA^-$ (2), $I2CA^-$ (1), I2CA(1), and I2CA(2). For each structure with the exception of I2CA(1), each method correctly predicts two low-lying electronic transitions: a ^1L_a and a ^1L_b transition. The ^1L_b transition is lower in energy, followed by the ^1L_a transition. (The justification for the labeling of these states is discussed below in Transition Densities.)

Predicted transition energies from ZINDO are all within 0.4 eV of the experimental results for the ^1L_a, ^1L_b, and ^1B transitions for each molecule. For TDDFT, the BLYP functional was found to be more accurate than the B3LYP functional in predicting transition energies, and the accuracy increased with increasing basis set size. The 6-31G** basis with the BLYP functional yielded transition energies all within 0.5 eV of experiment for aniline, indoline, $I2CA^-$ (1), and $I2CA^-$ (2). The accuracy of the B3LYP functional also increased with increasing basis. With the 6-31G** basis, predicted B3LYP transition energies were all within 0.75 eV of experiment. These results are consistent with previous reports that place transition energies given by TDDFT within approximately 0.3 eV of experimental values.[5,25,42,43] The energy of the predicted electronic transitions for neutral structures I2CA(1) and I2CA(2) also correspond well with experimental transition energies.

Following a trend commonly seen,[1,25] CIS overestimates the transition energy with each basis set used. The energies are overestimated by 1 eV for the ^1L_b and ^1L_a transitions and by nearly 2 eV for the ^1B transitions. This method also places the ^1L_b and ^1L_a transition within 0.4 eV of each other for each molecule studied. Results improve somewhat upon increasing basis set size from 6-31G to 6-31G*.

Excited-State Dipole Moments. Excited-state dipole moments are listed in Table 4. The BLYP functional predicts a lower dipole moment for the ^1L_b state of aniline (1.69 D) than for the ^1L_a state (3.62 D). This trend is repeated for indoline (2.05 vs 3.31 D), $I2CA^-$ (1) (2.47 vs 3.30 D), $I2CA^-$ (2) (2.37 D vs 3.94 D), and I2CA(2) (1.95 vs 3.31 D). A larger dipole moment of the ^1L_a state due to a larger charge-transfer component of electron density has also been observed for indole.[44] I2CA(1) does not follow the same trend as the other structures. The four lowest electronic states have dipole moments that are similar, with only transition three having a significantly higher dipole moment than the others.

Excited-State Configurations. The BLYP/6-31G** configurations from TDDFT for the ^1L_b and ^1L_a transitions for the molecules studied are shown in Table 4. The ^1L_b band of aniline and indoline is characterized predominately by a HOMO−LUMO transition with, to a lesser extent, a contribution from a

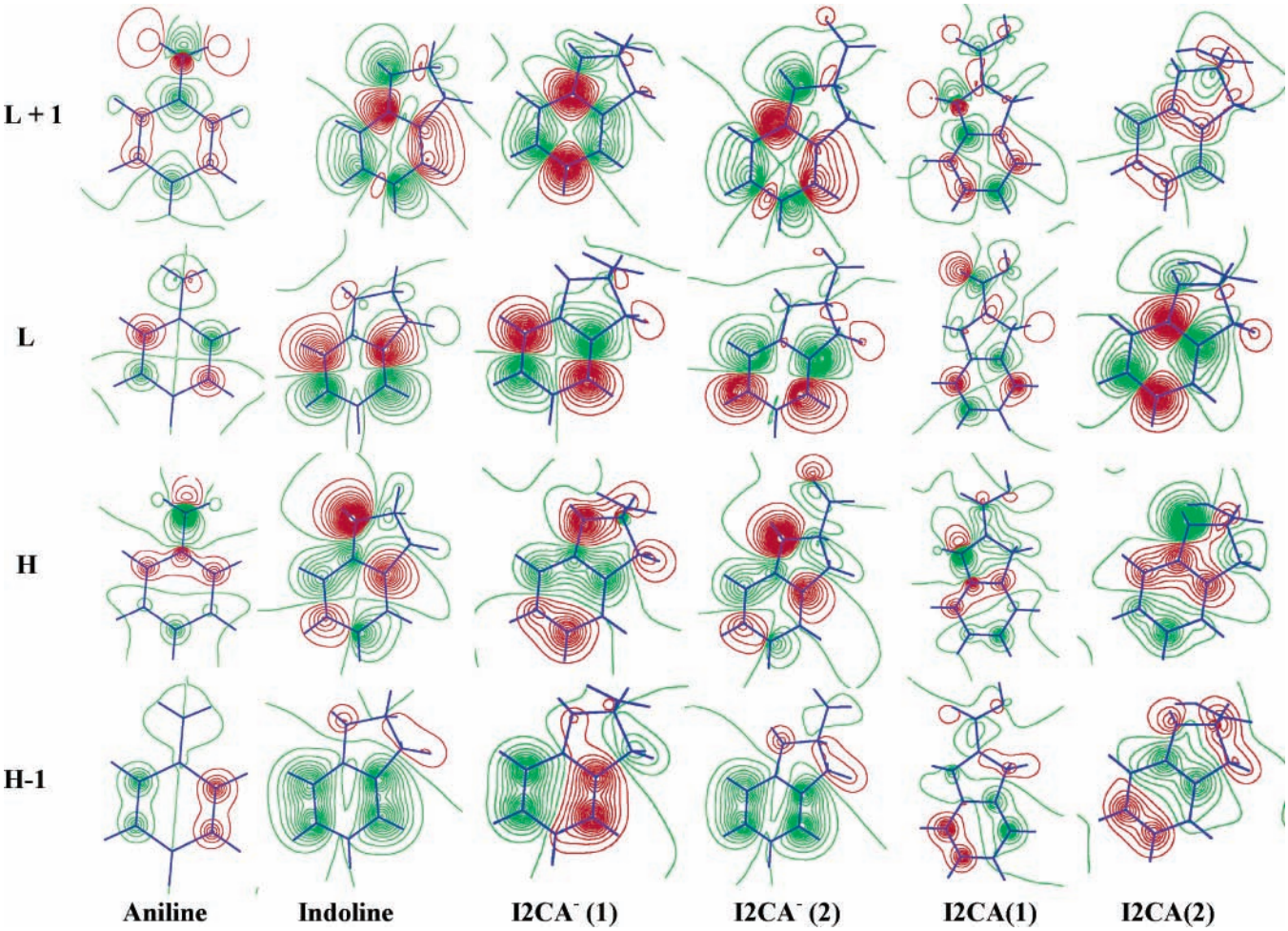

Figure 2. Molecular orbitals for (left to right) aniline, indoline, $I2CA^-$ (1), $I2CA^-$ (2), I2CA(2), and I2CA(1) (generated from the BLYP functional and the 6-31G* basis set). The orbitals are ordered (bottom to top) HOMO−1, HOMO, LUMO, LUMO+1. Orbital plots were generated using Molden[31] with a contour interval of 0.015.

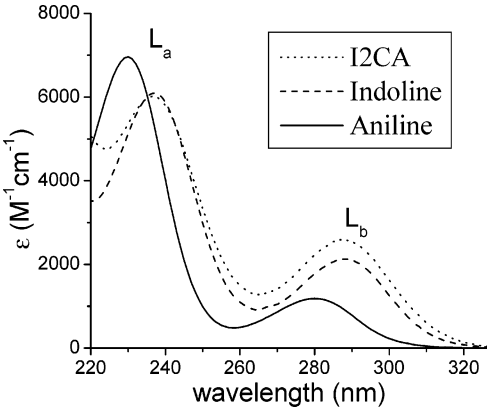

Figure 3. Absorption spectra of aniline, indoline, and I2CA in water.

HOMO−1 to LUMO+1 transition. The ^1L_a band consists of a HOMO to LUMO+1 and a HOMO−1 to LUMO transition. The excited-state configurations for aniline and indoline are remarkable similar, with only very small differences in the coefficients.

$I2CA^-$ (1) and $I2CA^-$ (2) are similar to indoline and aniline in that the HOMO−LUMO configuration still dominates the ^1L_b transition and the HOMO−LUMO+1 configuration dominates the ^1L_a transition. It may be noted that the HOMO−1 to LUMO+1 contribution to the ^1L_a transition and the HOMO−1 to LUMO contribution to the ^1L_b transition are reversed in sign for $I2CA^-$ (2) compared to $I2CA^-$ (1). This is a consequence of parity reversals in lobes of the HOMO−1, HOMO, and LUMO+1 orbitals of $I2CA^-$ (2) relative to those of $I2CA^-$ (1) (Figure 2).

The transition configurations for I2CA(2) do not differ significantly from those for aniline and indoline. In I2CA(1), the second electronic transition is dominated by HOMO−LUMO, and the fourth transition is dominated by HOMO−LUMO+1, but as will be discussed in Transition Densities, these transitions do not correspond well to a ^1L_b or ^1L_a designation.

It is worth noting that the orbital designations defining the ^1L_a and ^1L_b transitions for the molecules studied here differ from those previously found for indole. CIS and semiempirical calculations of the excited states of indole[13,14] predict that the HOMO to LUMO excitation of indole dominates the ^1L_a transition and the HOMO−1 to LUMO excitation dominates the ^1L_b transition. An examination of the CIS orbitals involved in the ^1L_a and ^1L_b transitions of indole[13] compared to the DFT orbitals of indoline shows a strong correlation between the HOMO of indoline and the HOMO−1 of indole and between the HOMO−1 of indoline and the HOMO of indole. In other words, similar orbitals are involved in the ^1L_a and ^1L_b transitions for both indoline and indole, but the two highest occupied orbitals have been switched in energy. The fact that these orbitals are reversed in energy between indoline and indole, which differ only by the presence of a double bond in the five-membered ring of indole, appears to be responsible for the overlap of the

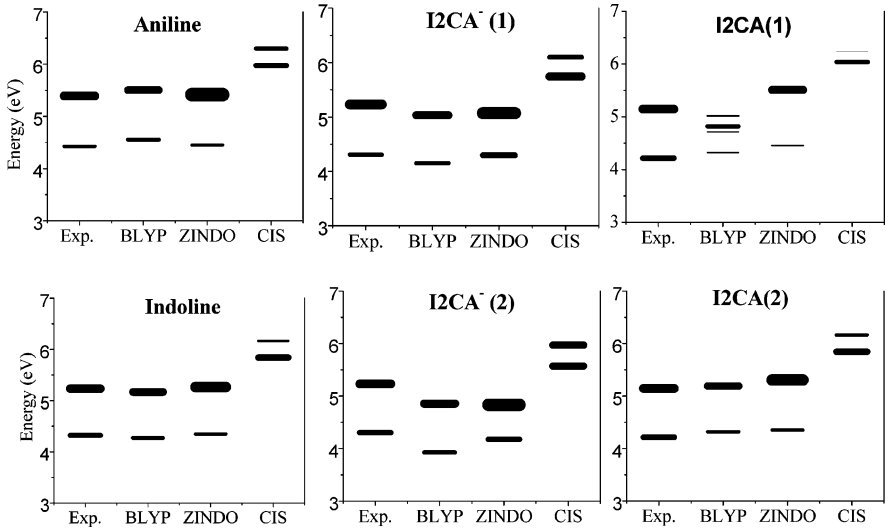

Figure 4. Summary of results. Experimental, BLYP/6-31G**, CIS/6-31G*, and ZINDO results are listed. Excitation energies are in electronvolts. Band thickness is a function of oscillator strength. For I2CA$^-$ and I2CA, the experimental oscillator strengths and transition energies shown for each conformation represent an average over all of the conformations present in solution.

^1L_a and ^1L_b states in indole, whereas these states are well separated in indoline.

Spectroscopic Transition Properties. Oscillator Strengths. Calculated oscillator strengths are given in Table 3 and are represented by the thickness of the bands in Figure 4. The most notable finding is the remarkable accuracy of TDDFT in predicting oscillator strengths for most of the molecules studied. Neither functional employed appears to outperform the other consistently because BLYP is more accurate for aniline and B3LYP is more accurate for indoline. TDDFT remains accurate in predicting oscillator strengths for the acid structures. The oscillator strengths predicted for I2CA$^-$ (1) even seem to reflect the observed state mixing (see Transition Densities), which is evidenced by an increase in the ^1L_b oscillator strength and a decrease in the ^1L_a oscillator strength. TDDFT does not predict oscillator strengths close to experimental values for I2CA(1), instead predicting the presence of a number of very weak transitions. The lengthening of the C1−N bond in I2CA(1) (Table 1) and the loss of resonance between the aromatic ring and the nitrogen are likely responsible for the decrease in oscillator strength predicted by these theoretical methods for this molecule. At the same time, this loss of resonance with the aromatic ring does not seem to reduce the contribution from the five-membered ring and the carboxyl group to the electronic transitions (see Transition Dipoles). It should be noted that in solution, whether aqueous or nonaqueous, at least two conformations appear to coexist for I2CA$^-$ and I2CA. The obtained experimental oscillator strength is a weighted average of the oscillator strength of each structure present. It is therefore not entirely accurate to compare quantitative theoretical results directly for a single structure with experimental results that include a mixture of two or more structures. This being said, the theoretical methods used here do an effective job of calculating oscillator strengths for the acid structures.

ZINDO is adequate in predicting the oscillator strength of the ^1L_b transition for these molecules. ZINDO overestimates the oscillator strength for the ^1L_a and ^1B transitions for each molecule by up to 50 and 100%, respectively. Unlike TDDFT, ZINDO predicts the presence of a ^1L_b and a ^1L_a transition for I2CA(1); however, it drastically underestimates the ^1L_b oscillator strength. CIS predicts the ^1L_b transition to be significantly stronger than the ^1L_a in aniline, indoline, I2CA$^-$ (1), and I2CA(2), but in I2CA$^-$ (2), the two are predicted to be nearly equal.

Calculations predict that the I2CA(1) structure is lower in energy than I2CA(2), although this energy difference is decreased by simulating solvent effects with Tomasi's polarized continuum model.[45] In addition, fluorescence lifetime measurements of I2CA in nonaqueous solutions are dominated by a fast fluorescence lifetime that is attributed to the hydrogen-bonded structure.[8] However, the absorption spectrum of I2CA in acetonitrile (not shown) and the experimental oscillator strength of I2CA match more closely the TDFDT results for I2CA(2) than I2CA(1). On the basis of experimental fluorescence lifetime results[8] and the calculated energies of the structures, it seems most likely that I2CA(1) is the predominant form and TDDFT has overestimated the extent of state mixing (see Transition Densities), leading to predicted oscillator strengths for I2CA(1) that are not as accurate as for the other structures.

Transition Densities. The definitions of the ^1L_a and ^1L_b states of aromatic molecules originate with the differences in the transition densities to these states. The ^1L_a electronic state is generally characterized as one that possesses transition density that is centered on the atoms, and the ^1L_b electronic state possesses transition density that is centered between atoms.[12]

The differences in ^1L_a and ^1L_b transition densities have been predicted theoretically. Using the spectroscopic version of the intermediate neglect of differential overlap (INDO-S-SCI), Callis found that for indole the transition density to the ^1L_a state involved mostly atomic regions and the ^1L_b transition density was centered between atoms.[14]

For the relevant electronic excitations of aniline, indoline, I2CA$^-$ (1), I2CA$^-$ (2), I2CA(1), and I2CA(2), the transition density from the ground to the excited state was calculated (Figures 5 and 6). TDDFT directly calculates transition density from the response of the ground-state electron density to a dynamic electric field The reported transition density corresponds to the spatial shift in electron density that arises from the electronic excitation. It is computed at the random-phase approximation level using TDDFT methodology implemented in Gaussian 98. The electronic transitions of aniline have been used here as a basis of comparison for indoline and I2CA. The ^1L_a and ^1L_b transitions of aniline have been well studied elsewhere.[46−49]

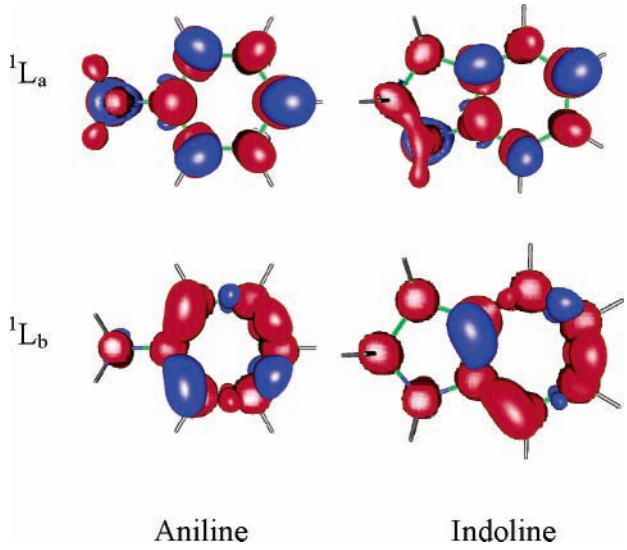

Figure 5. Transition densities for aniline and indoline. The bottom and top rows display the transition density for the ^1L_b and ^1L_a transitions, respectively. Transition densities were calculated at the random-phase approximation level and correspond to the spatial shift in electron density upon excitation.

The transition densities to the first and second electronic excited states of aniline and indoline display clearly the difference in the ^1L_a and ^1L_b states. The first electronic transition of aniline has been well documented as a ^1L_b state. The transition density to the first excited state of indoline matches closely that of aniline in that the transition density is centered between atoms (Figure 5). The electronic transition to the second excited state of aniline, known to be the ^1L_a state, contains nodes on the bonds and density on the atoms. The transition density to this state for indoline also contains nodes on the bonds and density on the atoms. Thus, the presence of the five-membered ring in indoline does not appear to change the nature of the lowest electronic states. The lowest-energy electronic transition for indoline is clearly ^1L_b in nature, and the second transition is ^1L_a in nature.

In the case of anionic acid structures I2CA$^-$ (1) and I2CA$^-$ (2), there appears to be a slight mixing of ^1L_a and ^1L_b character in the two lowest excited states (Figure 6). The transition densities for the second state of I2CA$^-$ (2) and I2CA$^-$ (1) are consistent with ^1L_a character. However, the transition densities to the first excited state for these molecules appear to contain some ^1L_a character. The most significant example of this is the decrease in transition density between carbon atoms C2 and C3. (See Figure 1 for atom numbering.) The transition density between atoms C5 and C6 has also changed significantly for I2CA$^-$ (2) and I2CA$^-$ (1) relative to that of indoline and aniline.

The transition densities for I2CA(2) appear to possess nearly pure ^1L_b and ^1L_a character. However, the mixing observed with the anionic acid structures is even more evident in the case of I2CA(1). The transition densities for the first four electronic excitations of I2CA(1) were calculated; the transition densities to the second and fourth are shown in Figure 6. The transition densities for I2CA(1) show that the electronic transitions for this molecule are not of a pure ^1L_a or ^1L_b nature. Transition densities to the first four states of this molecule do not resemble the transition densities of aniline and indoline in that there is no clear pattern of density on or between atoms for any of the states. Each state appears to have mixed ^1L_a and ^1L_b character. The observed features of I2CA can be explained by increased mixing between the ^1L_a and ^1L_b states as the ring structure and then the carboxyl group is added to the aniline. The mixing of the ^1L_a and ^1L_b states in indoline and I2CA is due to the reduced symmetry in the system and is likely exacerbated in I2CA by the presence of the polarizing carboxyl group.

Transition Dipoles. Transition dipoles for the ^1L_b and ^1L_a transitions of aniline, indoline, I2CA$^-$ (2), I2CA$^-$ (1), and I2CA(2), were calculating using TDDFT with the BLYP functional and the 6-31G* basis set (Figure 7). The blue arrow represents the dipole for the ^1L_a transition; red represents the ^1L_b transition. Transition dipoles for the second (red) and the fourth (blue) transitions of I2CA(1) are also shown. The origin of the arrow in each case is the center of mass, the direction corresponds to the orientation of the dipole, and the arrow length is proportional to the dipole's magnitude. From the center of mass, the *x* and *y* axes are in the plane of the aromatic, and the *z* axis is normal to the plane of the aromatic.

The transition dipoles for aniline are very nearly coplanar with the molecule. In aniline, there is a negligible contribution in the *x* axis to the ^1L_b transition dipole and a zero contribution from the *z* axis (with the *z* axis coming out of the aromatic plane). The ^1L_a transition dipole has a zero contribution from the *y* axis and only a 0.0012 au contribution from the *z* axis. These deviations from orthogonal coplanarity in aniline are related to the slight deviation from C_{2v} symmetry.

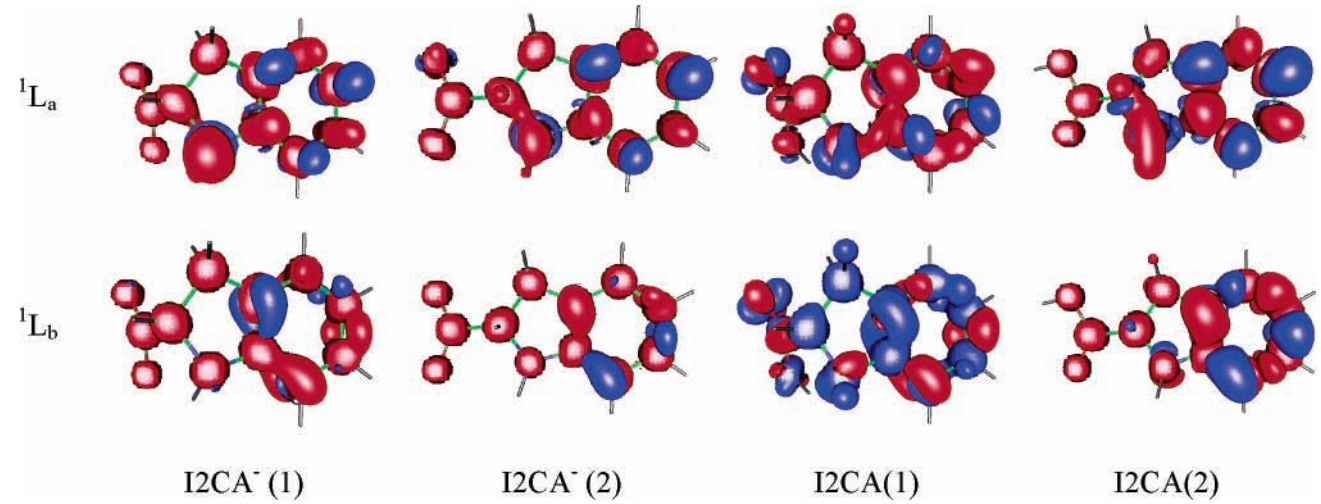

Figure 6. Transition densities for (left to right) I2CA$^-$ (1), I2CA$^-$ (2), I2CA(1), and I2CA(2). The bottom and top rows display the transition density for the ^1L_b and ^1L_a transitions, respectively. Transition densities were calculated at the random-phase approximation level and correspond to the spatial shift in electron density upon excitation.

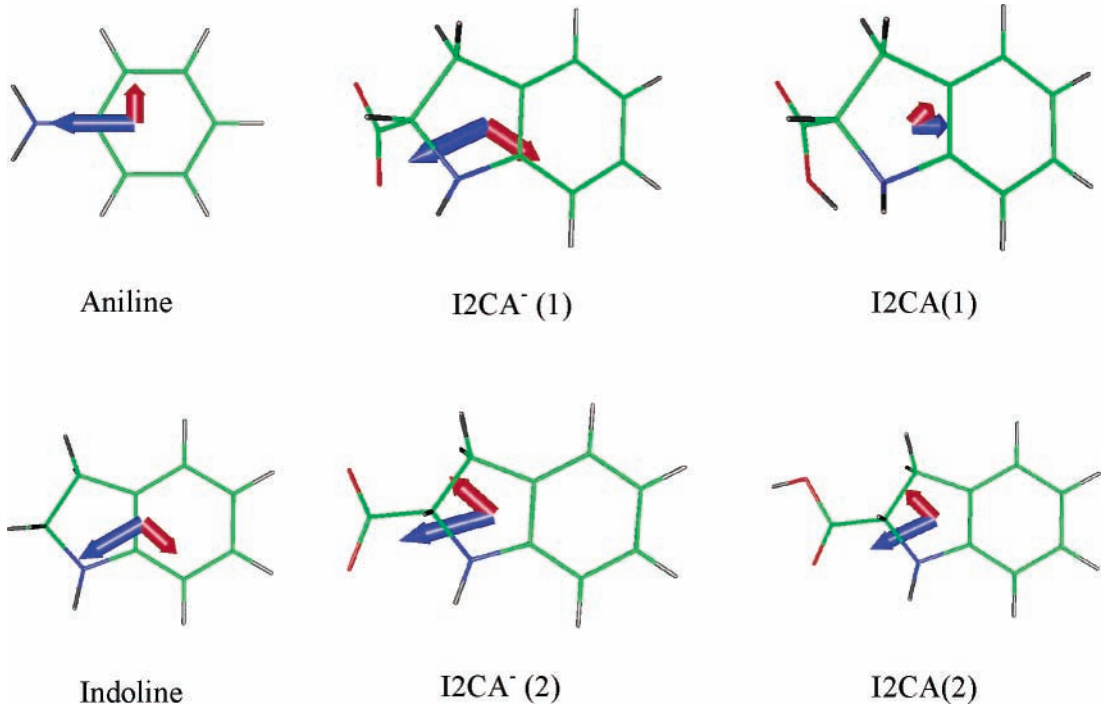

Figure 7. Transition dipoles (left to right) for (row 1) aniline, I2CA$^-$ (1), and I2CA(1) and (row 2) indoline, I2CA$^-$ (2), and I2CA(2). In red is the transition dipole for the ^1L_b transition; in blue is the transition dipole for the ^1L_a transition.

For indoline and the acid structures, the out-of-aromatic-plane contribution to the transition dipoles increases. For indoline, the ^1L_a transition dipole is nearly contained in the $x-y$ plane of the aromatic, with only a 0.0030 au contribution along the z axis. The ^1L_b transition dipole of indoline possesses a 0.038 au out-of-plane contribution. The ^1L_a transition dipole for I2CA$^-$ (2) possesses an out-of-aromatic-plane component (0.050 au) that is over an order of magnitude higher than the out-of-plane component for the ^1L_a transition of indoline. The ^1L_a transition dipole for I2CA$^-$ (1) contains an out-of-plane component (0.31 au) that is significantly higher than the out-of-plane component for the transition dipoles of the ^1L_a transition for the other molecules studied. The out-of-plane contribution for the ^1L_b transition dipole is 0.010 au for I2CA$^-$ (2) and 0.0880 au for I2CA$^-$ (1). The ^1L_b transition dipoles of indoline, I2CA$^-$ (2), and I2CA$^-$ (1) are oriented nearly parallel to the N−C8 bond. (See Figure 1 for atom numbering.) The ^1L_b dipoles for I2CA$^-$ (2) and I2CA$^-$ (1) are nearly parallel but are oriented in an opposite direction because of a large area of negative transition density centered on C6 for I2CA$^-$ (1).

The π-to-π^* transitions for planar aromatics are the result of electronic transitions between π and π^* orbitals that are strictly symmetric about the molecular plane. There would not be an out-of-plane component to the transition dipoles if this were strictly the case. In the case of all structures studied, the aromatic group is almost perfectly planar. The nonaromatic N and C atoms are displaced slightly from this plane. The π-to-π^* transitions involving aromatic carbons and atoms not in this plane could contribute to the transition dipole not lying in the same plane of the aromatic. A glance at the π orbitals (Figure 2) confirms that there is a significant contribution to the π-electron density for the π and π^* orbitals from the atoms of the five-membered ring, thus leading to transitions that are not perfectly parallel to the plane of the aromatic.

For the acid structures, there is additional π-electron density centered on the carboxyl group, which lies outside the aromatic plane. This density contributes to the out-of-aromatic-plane character of the transition dipole. The magnitude of the out-of-plane component in the transition dipoles could be indicative of the effect that this additional π-electron density has on the electronic transitions.

The transition dipoles of I2CA(1) give further insight into its electronic transitions. Close examination of the transition dipoles of I2CA(1) reveals a significant difference in the out-of-aromatic-plane component between these dipoles. Transition dipoles to the first and third states (not shown) have an order of magnitude greater out-of-plane component than the second and fourth dipoles. This suggests that the first and third transitions may involve more electron density from the acid group and may be less aromatic in nature than the second and fourth transitions. This information, combined with the excited-state configurations that show a HOMO−LUMO contribution to the second state and a HOMO−LUMO+1 dominance of the fourth state (Table 4), suggests that the second and fourth states of I2CA(1) may be more closely related to the ^1L_a and ^1L_b transitions of other indolines than the first and third transitions. A closer look at the excited-state configurations of I2CA(2) reveals that the orbitals contributing to the first and third transitions of I2CA(1) contribute only to *very weak* transitions in I2CA(2) (oscillator strengths of less than 0.003) (not shown). These orbitals are heavy in electron density in the area of the carboxyl group and appear to be further evidence of the effect of the contribution of the carboxyl group to the electronic structure. This contribution is much more prevalent in the I2CA(1) structure than in I2CA(2).

Relevance of Transition Dipoles to the Experiment. The ^1L_b transition dipoles of indoline and the two acid structures are of particular interest to the experiment because these are the states from which fluorescence occurs. It is important, therefore, to note the direction of the ^1L_b transition dipole relative to the bond (N−C8) between the nitrogen and the adjoining carbon on the five-membered ring for indoline and I2CA. Fluorescence polarization from indoline should be oriented roughly parallel to this axis in a peptide. The N−C8 bond becomes part of the peptide backbone when indoline is incorporated into a peptide. This bond is rigid; thus the

fluorescence polarization from the ^1L_b state will be oriented in a direction that is nearly parallel to this bond and, therefore, also parallel to the peptide backbone at this location in the peptide.

Also of importance to the experiment is the angle between the ^1L_b and ^1L_a transition dipoles. Aniline is very nearly symmetric and nearly planar; the angle between the dipoles was found to be 90°. For the remaining molecules studied, the nonplanarity of the five-membered ring and the contribution to the π-electron density from these atoms result in transition dipoles that are offset from 90°. The angle between the transition dipoles of indoline was calculated to be 108°. For both I2CA$^-$ (1) and I2CA$^-$ (2), this angle was calculated to be 58°. The angle between the dipoles for I2CA(2) was found to be 71°.

State Mixing: Theory versus Experiment. The absorbance spectra look similar as one progresses from aniline to indoline to I2CA (Figure 3). Upon closer inspection, there exists an increase in the extinction coefficient for the ^1L_b band along this series. A broadening of the ^1L_b band in the case of the acid and a decrease in the valley depth between the ^1L_a and ^1L_b absorption features are also evident. The gradual mixing of the ^1L_a and ^1L_b states is detectable theoretically as an increase in the oscillator strength of the ^1L_b absorption feature relative to that of ^1L_a. TDDFT oscillator strengths using BLYP/6-31G** are reported in Table 4, with experimental values in parentheses. Experimentally, there is an 86% increase in the ^1L_b oscillator strength in going from aniline to indoline and a 115% increase from aniline to I2CA$^-$ (2). TDDFT predicts a 39% increase from aniline to indoline and a 73% increase in the ^1L_b oscillator strength from aniline to I2CA$^-$ (2). The increase in oscillator strength from aniline to I2CA$^-$ (1) is 96%.

Conclusions

An understanding of the properties of the ^1L_a and ^1L_b states of indoline and I2CA will facilitate their use as fluorescent probes. The ^1L_a and ^1L_b transitions for these two molecules occur in a wavelength range that is well suited to fluorescence studies. The two transitions are separated well enough that the preferential excitation of one over the other is easily achieved. In water, the ^1L_b and ^1L_a states of indoline absorb at 287 and 237 nm, respectively, with oscillator strengths of 0.049 and 0.16, respectively. For I2CA in water, the ^1L_b and ^1L_a states absorb at 288 and 237 nm, respectively. They have oscillator strengths of 0.056 and 0.16 (Figure 4 and Table 3), respectively. These wavelengths are red-shifted slightly in acetonitrile with a very small increase in oscillator strength.[8] Fluorescence from the ^1L_b state is polarized nearly parallel to the N−C8 bond. In a peptide, this bond will be part of the peptide backbone, a characteristic that will allow a straightforward analysis of information obtained by fluorescence depolarization.

Overall, TDDFT using either the B3LYP or BLYP functional outperforms both the ZINDO and CIS methods for the calculation of excitation energy and oscillator strength. For indoline, I2CA, and aniline, B3LYP and BLYP accurately predict excitation energies. Theoretical results from the 6-31G** basis range from within 0.08 to 0.70 eV of experiment. The accuracy of these functionals in predicting transition energies for indoline, I2CA, and aniline is consistent with that of similar systems.[42,50]

The accuracy of the predicted oscillator strengths is a bit more surprising. Again, looking at the 6-31G** basis, the predicted ^1L_b transitions of I2CA$^-$ (2) from B3LYP and aniline from BLYP differ by less than 7 and 5%, respectively, from experiment. Errors range up to nearly 35% but do not exceed this percentage.

The calculations presented in this study have enabled us to assign the ^1L_b and ^1L_a transitions of indoline and I2CA. The electronic transitions of indoline are very similar to those of aniline. Two charged acid structures were analyzed, one of which is able to form a 2.0-Å hydrogen bond between atoms O2 and H1. In the case of the acid structures, the π-electron density on the carboxyl group causes a slight mixing in the ^1L_a and ^1L_b states, as demonstrated by the transition densities, and an increase in the predicted oscillator strength for the ^1L_b state.

The electronic properties of I2CA are of particular interest for predicting the nature of the electronic states for indoline incorporated into peptides. It is possible that placing indoline into a peptide with carbonyl groups on each side of the ring may cause further mixing. Even with an increase in state mixing, it is likely that the fluorescence properties of indoline when inserted into a peptide will remain characteristic of the ^1L_b states of indoline.

Acknowledgment. B.D.S. acknowledges support from a training grant in Dynamic Aspects of Chemical Biology (NIH 5 T32 GM08545-09). Acknowledgment is made to the donors of the Petroleum Research Fund, administered by the American Chemical Society for the support of this research.

References and Notes

(1) Foresman, J. B.; Head-Gordon, M.; Pople, J. A.; Frisch, M. J. *J. Phys. Chem.* **1992**, *96*, 135.
(2) Johnson, B. G.; Gill, P. M. W.; Pople, J. A. *J. Chem. Phys.* **1993**, *98*, 5612.
(3) Teppen, B. J.; Miller, D. M.; Cao, M.; Frey, R. F.; Newton, S. Q.; Momany, F. A.; Ramek, M.; Schaefer, L. *THEOCHEM* **1994**, *117*, 9.
(4) Casida, M. E. *Recent Adv. Comput. Chem.* **1995**, *1*, 155.
(5) Petersilka, M.; Gossmann, U. J.; Gross, E. K. U. *Phys. Rev. Lett.* **1996**, *76*, 1212.
(6) Johnson, C. K.; Bothwell, T. G.; Allen, M. W.; Osborn, K. D. *Biophys. J.* **2001**, *80*, 360a.
(7) Allen, M. W.; Bothwell, T. G.; Slaughter, B. D.; Johnson, C. K. *Biophys. J.* **2002**, *82*, 428a.
(8) Allen, M. W.; Unruh, J. R.; Slaughter, B. D.; Pyszczynski, S. J.; Hellwig, T. R.; Kamerzell, T. J.; Johnson, C. K. *J. Phys. Chem. A* **2003**, *107*, 5660.
(9) Allen, M. W.; Slaughter, B. D.; Larive, C. K.; Johnson, C. K. To be submitted for publication.
(10) Ross, J. B. A.; Rusinova, E.; Luck, L. A.; Rousslang, K. W. In *Topics in Fluorescence Spectroscopy*; Lacowicz, J. R., Ed.; Plenum Publishing: New York, 2000; Vol. 6, p 17.
(11) Klevens, H. B.; Platt, J. R. *J. Chem. Phys.* **1949**, *17*, 470.
(12) Platt, J. R. *J. Chem. Phys.* **1949**, *17*, 484.
(13) Slater, L. S.; Callis, P. R. *J. Phys. Chem.* **1995**, *99*, 8572.
(14) Callis, P. R. *J. Chem. Phys.* **1991**, *95*, 4230.
(15) Chabalowski, C. F.; Garmer, D. R.; Jensen, J. O.; Krauss, M. *J. Phys. Chem.* **1993**, *97*, 4608.
(16) Muino, P. L.; Callis, P. R. *J. Chem. Phys.* **1994**, *100*, 4093.
(17) Callis, P. R.; Burgess, B. K. *J. Phys. Chem. B* **1997**, *101*, 9429.
(18) Serrano-Andres, L.; Roos, B. O. *J. Am. Chem. Soc.* **1996**, *118*, 185.
(19) Anderson, W. P.; Edwards, W. D.; Zerner, M. C. *Inorg. Chem.* **1986**, *25*, 2728.
(20) Ridley, J.; Zerner, M. *Theor. Chim. Acta* **1973**, *32*, 111.
(21) Edwards, W. D.; Ohrn, N. Y.; Weiner, B. L.; Zerner, M. C. *Int. J. Quantum Chem., Quantum Chem. Symp.* **1984**, *18*, 507.
(22) Casida, M. E.; Jamorski, C.; Casida, K. C.; Salahub, D. R. *J. Chem. Phys.* **1998**, *108*, 4439.
(23) Runge, E.; Gross, E. K. U. *Phys. Rev. Lett.* **1984**, *52*, 997.
(24) Gross, E. K. U.; Kohn, W. *Adv. Quantum Chem.* **1990**, *21*, 255.
(25) Stratmann, R. E.; Scuseria, G. E.; Frisch, M. J. *J. Chem. Phys.* **1998**, *109*, 8218.
(26) Frisch, M. J.; Trucks, G. W.; Schlegel, H. B.; Scuseria, G. E.; Robb, M. A.; Cheeseman, J. R.; Zakrzewski, V. G.; Montgomery, J. A., Jr.; Stratmann, R. E.; Burant, J. C.; Dapprich, S.; Millam, J. M.; Daniels, A. D.; Kudin, K. N.; Strain, M. C.; Farkas, O.; Tomasi, J.; Barone, V.; Cossi, M.; Cammi, R.; Mennucci, B.; Pomelli, C.; Adamo, C.; Clifford, S.; Ochterski, J.; Petersson, G. A.; Ayala, P. Y.; Cui, Q.; Morokuma, K.; Malick, D. K.; Rabuck, A. D.; Raghavachari, K.; Foresman, J. B.; Cioslowski, J.; Ortiz, J. V.; Stefanov, B. B.; Liu, G.; Liashenko, A.; Piskorz, P.; Komaromi, I.; Gomperts, R.; Martin, R. L.; Fox, D. J.; Keith, T.; Al-Laham, M. A.; Peng, C. Y.; Nanayakkara, A.; Gonzalez, C.; Challacombe, M.; Gill, P. M.

W.; Johnson, B. G.; Chen, W.; Wong, M. W.; Andres, J. L.; Head-Gordon, M.; Replogle, E. S.; Pople, J. A. *Gaussian 98*; Gaussian, Inc.: Pittsburgh, PA, 1998.
(27) Petersson, G. A.; Al-Laham, M. A. *J. Chem. Phys.* **1991**, *94*, 6081.
(28) Ditchfield, R.; Hehre, W. J.; Pople, J. A. *J. Chem. Phys.* **1971**, *54*, 724.
(29) Lee, C.; Yang, W.; Parr, R. G. *Phys. Rev. B: Condens. Matter* **1988**, *37*, 785.
(30) Becke, A. D. *J. Chem. Phys.* **1993**, *98*, 5648.
(31) Schaftenaar, G.; Noordik, J. H. *J. Comput.-Aided Mol. Des.* **2000**, *14*, 123.
(32) Laaksonen, L. *J. Mol. Graphics* **1992**, *10*, 33.
(33) Bergman, D. L.; Laaksonen, L.; Laaksonen, A. *J. Mol. Graphics* **1997**, *15*, 301.
(34) Metzler, C. M.; Cahill, A. E.; Petty, S.; Metzler, D. E.; Lang, L. *Appl. Spectrosc.* **1985**, *39*, 333.
(35) Siano, D. B.; Metzler, D. E. *J. Chem. Phys.* **1969**, *51*, 1856.
(36) Metzler, D. E.; Harris, C. M.; Johnson, R. J.; Saino, D. B.; Thomson, J. A. *Biochemistry* **1973**, *12*, 5377.
(37) Mulliken, R. S.; Rieke, C. A. *Phys. Soc. Rep. Prog. Phys.* **1941**, *8*, 231.
(38) Jiang, J. C.; Lin, C. E. *THEOCHEM* **1997**, *392*, 181.
(39) Fukuyo, M.; Hirotsu, K.; Higuchi, T. *Acta Crystallogr., Sect. B* **1982**, *38*, 640.
(40) Wang, Y.; Saebo, S.; Pittman, C. U., Jr. *THEOCHEM* **1993**, *100*, 91.
(41) Lister, D. G.; Tyler, J. K.; Hoeg, J. H.; Larsen, W. *J. Mol. Struct.* **1974**, *23*, 253.
(42) Hirata, S.; Lee, T. J.; Head-Gordon, M. *J. Chem. Phys.* **1999**, *111*, 8904.
(43) Hsu, C.-P.; Hirata, S.; Head-Gordon, M. *J. Phys. Chem. A* **2001**, *105*, 451.
(44) Callis, P. R. *Methods Enzymol.* **1997**, *278*, 113.
(45) Miertus, S.; Scrocco, E.; Tomasi, J. *Chem. Phys.* **1981**, *55*, 117.
(46) Petruska, J. *J. Chem. Phys.* **1961**, *34*, 1120.
(47) Bhat, B. S.; Sindhi, P. C.; Sanwari, R.; Bhat, C. V. *Orient. J. Chem.* **1986**, *2*, 24.
(48) Korter, T. M.; Borst, D. R.; Butler, C. J.; Pratt, D. W. *J. Am. Chem. Soc.* **2001**, *123*, 96.
(49) Kassab, E.; Evleth, E. M. In *The Role of Rydberg States in Spectroscopy and Photochemistry*; Sándory, C., Ed.; Kluwer Academic Publishers: Dordrecht, The Netherlands, 1999; Vol. 20, p 231.
(50) Jamorski, C.; Foresman, J. B.; Thilgen, C.; Luthi, H.-P. *J. Chem. Phys.* **2002**, *116*, 8761.